Metabolomics Analyses of Mouse Retinas in Oxygen-Induced Retinopathy

Yedi Zhou,[1,2] Wei Tan,[1,2] Jingling Zou,[1,2] Jian Cao,[1,2] Qian Huang,[1,2] Bing Jiang,[1,2] Shigeo Yoshida,[3] and Yun Li[1,2]

[1]Department of Ophthalmology, The Second Xiangya Hospital, Central South University, Changsha, Hunan, China
[2]Hunan Clinical Research Center of Ophthalmic Disease, Changsha, Hunan, China
[3]Department of Ophthalmology, Kurume University School of Medicine, Kurume, Fukuoka, Japan

Correspondence: Yun Li, Department of Ophthalmology, The Second Xiangya Hospital, Central South University, Changsha, Hunan 410011, China; yun.li@csu.edu.cn.

Received: September 28, 2020
Accepted: July 20, 2021
Published: August 10, 2021

Citation: Zhou Y, Tan W, Zou J, et al. Metabolomics analyses of mouse retinas in oxygen-induced retinopathy. *Invest Ophthalmol Vis Sci.* 2021;62(10):9. https://doi.org/10.1167/iovs.62.10.9

Purpose. Retinal neovascularization is a severe pathological process leading to irreversible blindness. This study aims to identify the altered metabolites and their related pathways that are involved in retinal neovascularization.

Methods. To reveal the global metabolomic profile change in the retinal neovascularization process, an untargeted metabolomics analysis of oxygen-induced retinopathy (OIR) mice retinas was carried out first, followed by the validation of amino acids and their derivatives through a targeted metabolomics analysis. The involved pathways were predicted by bioinformatic analysis.

Results. By untargeted metabolomics, a total of 58 and 49 metabolites altered significantly in OIR retinas under cationic and anionic modes, respectively. By bioinformatics analysis, "ABC transporters," "central carbon metabolism in cancer." and "alanine, aspartate, and glutamate metabolism" were the most enriched Kyoto Encyclopedia of Genes and Genomes (KEGG) pathways associated with the changed metabolites. By targeted metabolomics, no significant change was found in the assessed amino acids and their derivatives at postnatal day (P) 12, whereas significantly altered amino acids and their derivatives were recognized at P13, P17, and P42 in OIR retinas.

Conclusions. The metabolomic profile was significantly altered in the neovascularized retinas. In particular, numerous amino acids and their derivatives were significantly changed in OIR retinas. These altered metabolites, together with their associated pathways, might be involved in the pathogenesis of retinal neovascular diseases.

Keywords: amino acid, metabolomics, retinal neovascularization, oxygen-induced retinopathy (OIR)

Ocular neovascularization is a shared pathogenesis in numerous blinding diseases, including retinal neovascular diseases, such as proliferative diabetic retinopathy (PDR), retinal vein occlusion (RVO), retinopathy of prematurity (ROP), etc.[1] These retinal neovascular diseases are all leading causes of global blindness and have major impacts on human health and quality of life. Although antivascular endothelial growth factor (VEGF) therapy sheds new light on the treatment of retinal neovascular diseases,[2] systemic and local side effects of anti-VEGF therapy cannot be ignored.[3,4] Furthermore, anti-VEGF agents have no or limited effect on some patients with ocular neovascular diseases. Thus, it is necessary to reveal deeper regulatory mechanisms of retinal neovascularization.

As a commonly recognized animal model used to study retinal neovascular diseases in vivo, the oxygen-induced retinopathy (OIR) model is established by exposing newborn pups to a hyperoxia environment,[5,6] which has been considered similar to the pathological process of ROP.[7] Through transcriptomics research, we previously identified differentially expressed mRNAs,[5] microRNAs,[8] long noncoding RNAs,[5] circular RNAs,[9] and tRNA-derived small RNAs[10] in the retinal tissues of OIR mouse model. Moreover, novel molecular networks and potential therapeutic targets were discovered by proteomic analysis in the OIR model.[11–13] However, the mechanism of pathological retinal neovascularization remains unclear.

As the final products of enzymatic processes, metabolites reflect physiological and pathological functions and activities from cells to tissues.[14] Metabolomics analyses are commonly used to identify the pathological process of diseases through identifying networks of metabolic profiles.[15] Recent studies reported that metabolomics revealed novel diagnostic biomarkers in cancer,[16] anxiety disorders,[17] osteoporosis,[18] and ocular diseases.[19] Metabolomics has been utilized in the study of extracellular vesicles,[20] genetic testing,[21] and mechanical investigation of macrophages.[22]

Recent studies also revealed the alteration of metabolites in several ocular disorders, such as diabetic retinopathy,[23] central retinal vein occlusion,[24] Vogt-Koyanagi-Harada disease,[25] macular neurodegenerative disease,[26] and

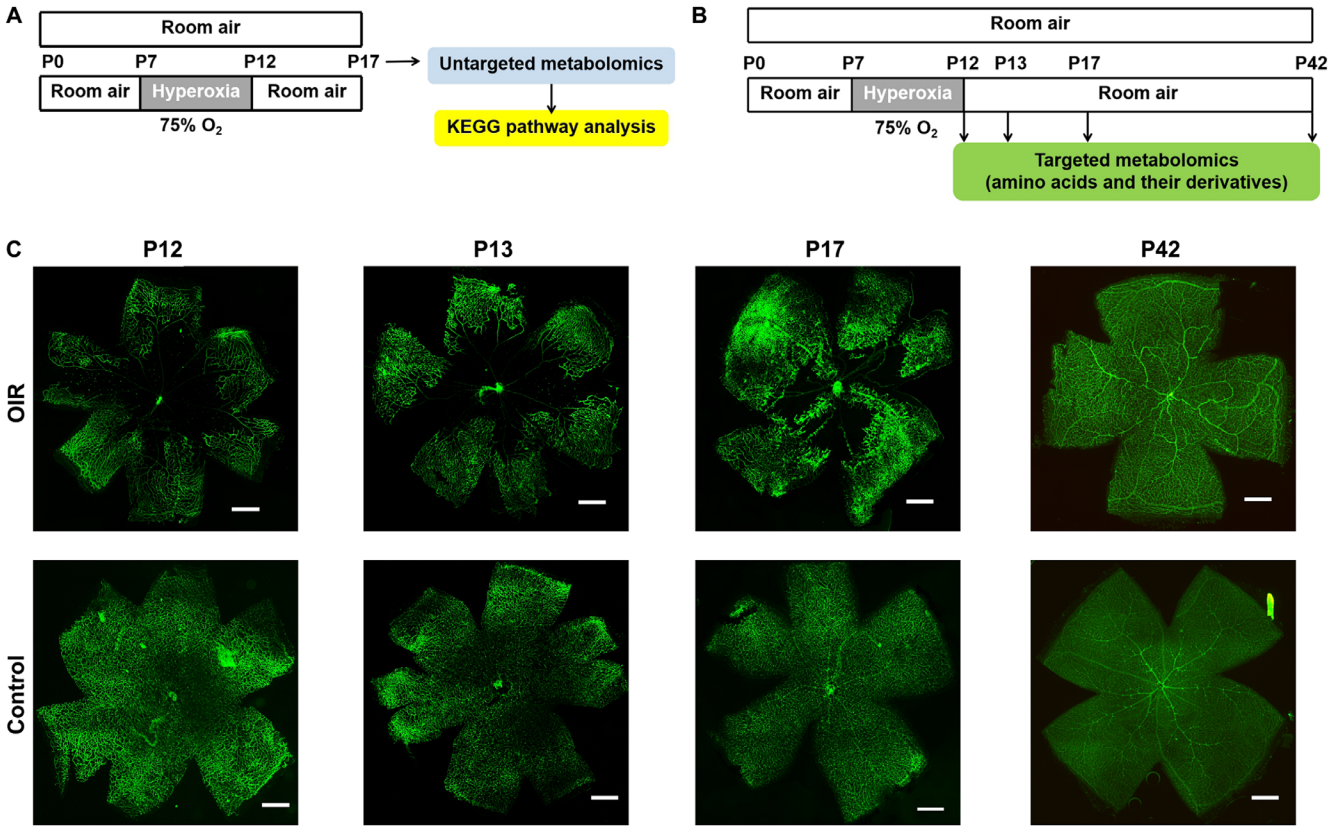

Figure 1. Establishment of OIR mouse model. Flowchart of the current experimental design: untargeted metabolomics analysis (**A**) and targeted metabolomics analysis of amino acids and their derivatives (**B**). Representative images of the flat-mounted retinas of OIR mice and control mice (**C**): the retinas of P12, P13, P17, and P42 mice were immunofluorescent stained by fluorescein-labeled isolectin B4. Scale bars = 500 µm.

age-related macular degeneration.[27] The plasma metabolomic alteration in OIR rats was identified by Lu et al., and they revealed that components of the "arginine and proline metabolism" pathway could be possible biomarkers in diagnosing patients with ROP.[28] By using untargeted metabolomics analysis, we recently examined the plasma metabolites in clinical samples from patients with treatment-requiring ROP and revealed numerous potential biomarkers that could be considered for future clinical applications.[29] Both studies demonstrated the altered metabolites in circulation, which indicated the systemic metabolic changes in neovascularized retinopathies. However, circulating blood is a more indirect reflection of the pathological process of the neovascular retinopathy, in this study, we investigate metabolomic profile in the retinal tissues of OIR in vivo, which hopefully would give more direct information on the pathogenesis, pathophysiology, and/or prognosis of retinal neovascularization.

In this study, through untargeted metabolomics analysis, the global metabolomic profile change in the retinal tissues of OIR mice was explored, and then by targeted metabolomics analysis, the changes of amino acids and their derivatives were validated. The involved pathways were predicted by bioinformatics analysis. The experimental design of the metabolomics analyses is shown in Figures 1A, 1B.

Materials and Methods

Animal Ethics and the Mouse Model of Oxygen-Induced Retinopathy

C57BL/6J mice (Hunan SJA Laboratory Animal, Changsha, China) were treated according to the ARVO Statement for the Use of Animals in Ophthalmic and Vision Research. This study's experimental procedures were approved by the Institutional Animal Care and Use Committee of Central South University.

The OIR model was induced in mice as previously described[6] by exposing newborn pups to an environment with 75% oxygen at postnatal day 7 (P7), and were returned to a room air environment at P12, whereas control mice have been kept in the room air environment continuously. Retinas of both groups were collected at P17 for untargeted metabolomics analysis, and at P12, P13, P17, and P42 for targeted metabolomics analysis.

To identify animal modeling success, a mouse was randomly chosen from each litter of both groups at P12, P13, P17, and P42. The flat-mounted retinas were immunofluorescent stained by fluorescein-labeled isolectinB4 (Vector Laboratories, Burlingame, CA, USA)[30] and were photographed by the fluorescent microscope DMI4000B (Leica, Wetzlar, Germany).

Sample Collection and Preparation

Retinas of both eyes were frozen and stored at −80°C immediately after the mice were euthanized at each time point. The mixture of retinas from two eyes of each mouse was one sample and 10 mg sample was adequately vortexed in a solution of cold methanol/ acetonitrile/H_2O. After ultrasonication and protein precipitation, the mixture was centrifuged for 20 minutes (14,000 g, 4°C) and dried in a vacuum centrifuge. Samples were re-dissolved in 100 µL solvent. To perform liquid-chromatography tandem mass spectrometry (LC-MS/MS) analysis, supernatants were collected. The standard curve was established for targeted metabolomics.

LC-MS/MS Analyses for Untargeted Metabolomics

The analyses were carried out by utilizing a UHPLC (1290 Infinity LC, Agilent Technologies, CA, USA) coupled to a quadrupole time-of-flight (AB SciexTripleTOF 6600). Using a 2.1 mm × 100 mm ACQUIY UPLC BEH 1.7 µm column (Waters, Ireland), samples were analyzed for HILIC separation. The parameters of the untargeted metabolomics can be referred to in our previous study.[29]

HPLC-MS/MS Analyses for Targeted Metabolomics

Utilizing a UHPLC (1290 Infinity LC; Agilent Technologies) coupled to a QTRAP (AB Sciex 5500), analyses of this study were performed. The mobile phase contained A = 25 mM CH3COONH4 + 0.08% FA in water and B = 0.1% FA in ACN. Samples were in the automatic sampler at 4°C, and the column temperatures were kept at 40°C constantly. The gradients were at a flow rate of 250 µL/min. A 4 µL aliquot of each sample was injected. The gradient was 90% B linearly reduced to 70% in 0–12 minutes, and then was reduced to 50% in 12–18 minutes and reduced to 40% in 18–25 minutes, and kept for 25–30 minutes. Then the B was raised to 90% in 30–30.1 minutes and kept for 30.1–37 minutes.

The quality control (QC) samples were applied to examine and evaluate the repeatability and stability and of this system. At the same time, the standard mixture of AA metabolites was set for the correction of chromatographic retention time.

In ESI cationic mode, settings of conditions were as below: Ion Source Gas1 (Gas1) as 40, Ion Source Gas2 (Gas2) as 40, curtain gas (CUR) as 30, source temperature: 500°C, IonSpray Voltage Floating (ISVF) ± 5500 V. Adopt the MRM mode detection ion pair.

Data Processing

For the untargeted metabolomics, using ProteoWizardMSConvert, the raw MS data (wiff.scan files) were converted to MzXML files before they were imported into freely available XCMS software. In the extracted ion features, only the variables with over 50% of the nonzero measurement values in at least one group were maintained. Through comparing the accuracy m/z value (<25 ppm), and tandem mass spectrometry (MS/MS) spectra with an in-house database (Shanghai Applied Protein Technology Co. Ltd., Shanghai, China) established with available authentic standards, the compound identification of metabolites was conducted.

For targeted metabolomics, the Multiquant software was applied for the extraction of chromatographic peak area and retention time. The AA standards correct retention time was applied to identify the metabolites.[31] Together with the biological samples, the quality control samples were processed. Detected metabolites in pooled samples with the coefficient of variation (CV) less than 30% were denoted as reproducible measurements.

Bioinformatics Analysis

Kyoto Encyclopedia of Genes and Genomes (KEGG) pathway analysis (https://www.kegg.jp/) was conducted to reveal the enriched pathways of the altered metabolites.

Statistical Analysis

For untargeted metabolomics, after normalized to total peak intensity, the processed data were uploaded before importing into SIMCA-P (version 14.1; Umetrics, Umea, Sweden) for multivariate data analysis. To assess the robustness of the model, the 7-fold cross-validation and response permutation testing was applied. In the OPLS-DA model, the variable importance in the projection (VIP) value of each variable was calculated to indicate its contribution to the classification. To measure the significance of each metabolite, metabolites with the VIP value >1 were further applied to Student's *t*-test at the univariate level, with a $P < 0.05$ or $P < 0.10$ as statistically significant. For targeted metabolomics of amino acids and their derivatives, metabolites with $P < 0.05$ were marked as notably altered metabolites.

Results

Untargeted Metabolomics of Retinal Tissues of OIR Mice and Controls

To evaluate the success of animal modeling of OIR, flat-mounted retinas of P12, P13, P17, and P42 mice of the same litters of both OIR model and control groups were immunofluorescent stained by isolectin B4, and typical pathological neovascular tufts and avascular areas were detected by representative images of OIR group, compared to the normal physiological vasculature of the retina in the control group (Fig. 1C).

To identify the differentially expressed metabolites in OIR retinas, 20 samples of retinas (10 OIR samples and 10 controls) at P17 were assessed for the initial untargeted metabolomics analysis. A total of 5899 cationic peaks and 4697 anionic peaks of metabolites were recorded according to the XCMS records.

As the principal component analysis (PCA) showed, in cationic and anionic modes, the QC samples gathered together closely (Figs. 2A, 2B), which indicated that the experiments have good repeatability. To determine the differences in metabolic profiles, OPLS-DA score plots were conducted to identify the metabolomic profile differences between these two groups. As demonstrated in Figures 2C and 2D, remarkable separations of the OIR group and control group were recognized in both cationic and anionic modes. Then, the permutation analysis of the OPLS-DA model was performed, and results indicated that the OPLS-DA model fitting was valid and stable in both ion modes (Figs. 2E, 2F).

Volcano Plot analysis has been applied to screen potential alteration of the metabolites following the criteria of fold change (FC) > 1.5 and $P < 0.05$. Identified altered metabolites with the criteria between these two groups (red points) under cationic mode (Fig. 3A) and anionic mode (Fig. 3B).

Investigative Ophthalmology & Visual Science

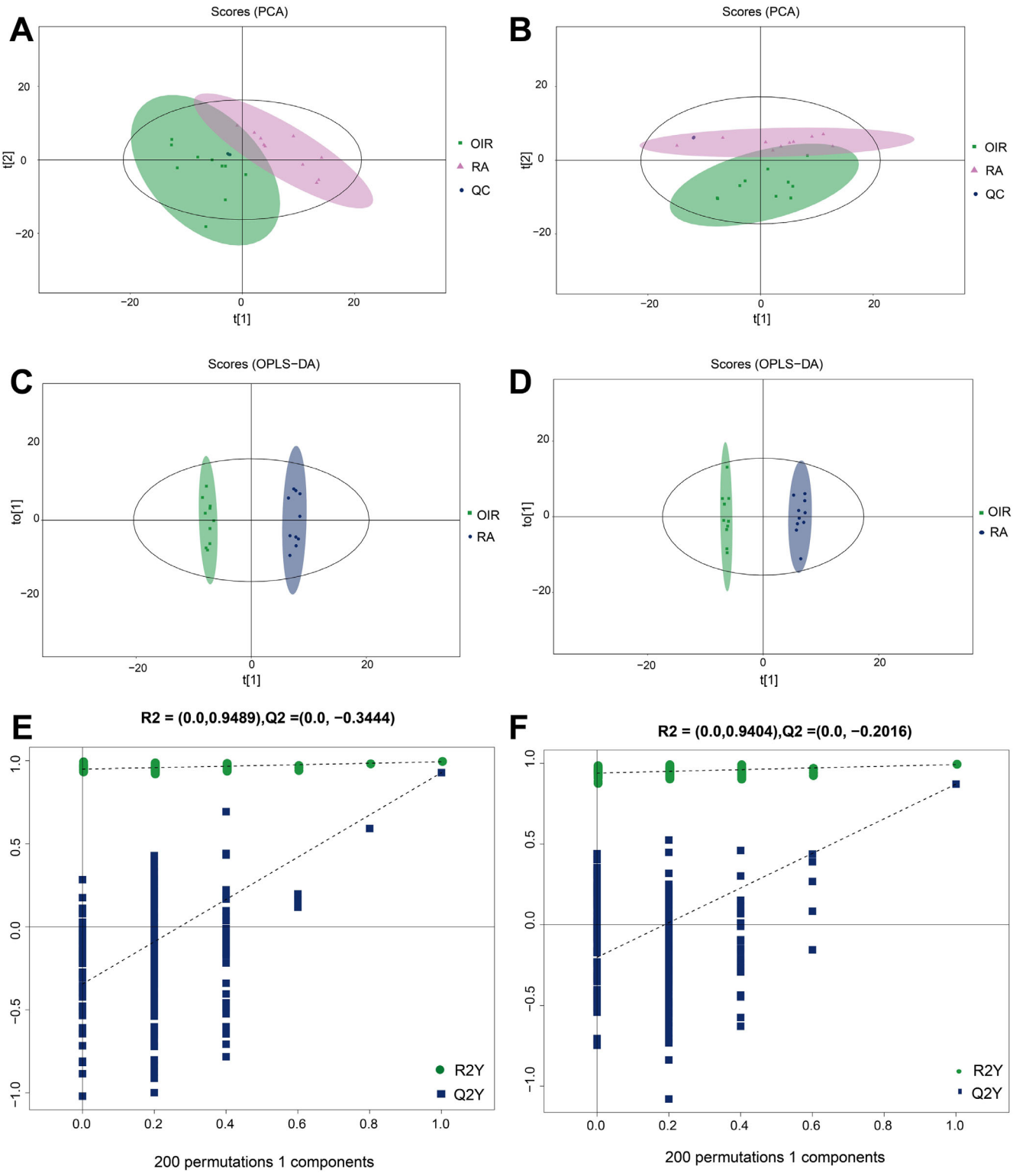

Figure 2. Qualification evaluation of untargeted metabolomics analysis. PCA analysis of the included samples in both groups under the cationic (**A**) and anionic mode (**B**). OPLS-DA score plot of OIR group and control group under the cationic (**C**) and anionic mode (**D**). Permutation analysis plot of the OPLS-DA model, under the cationic (**E**) and anionic mode (**F**).

Subsequently, the significantly changed metabolites under the criteria of VIP > 1 and $P < 0.1$ were selected and finally recognized after been compound identification with the database. Under the cationic mode, 58 altered metabolites (52 of them met $P < 0.05$) were recognized significantly difference (Fig. 4, Table 1). Particularly, between the two groups, there were 14 altered amino acids and their derivatives. On the other hand, 49 metabolites (45 of them

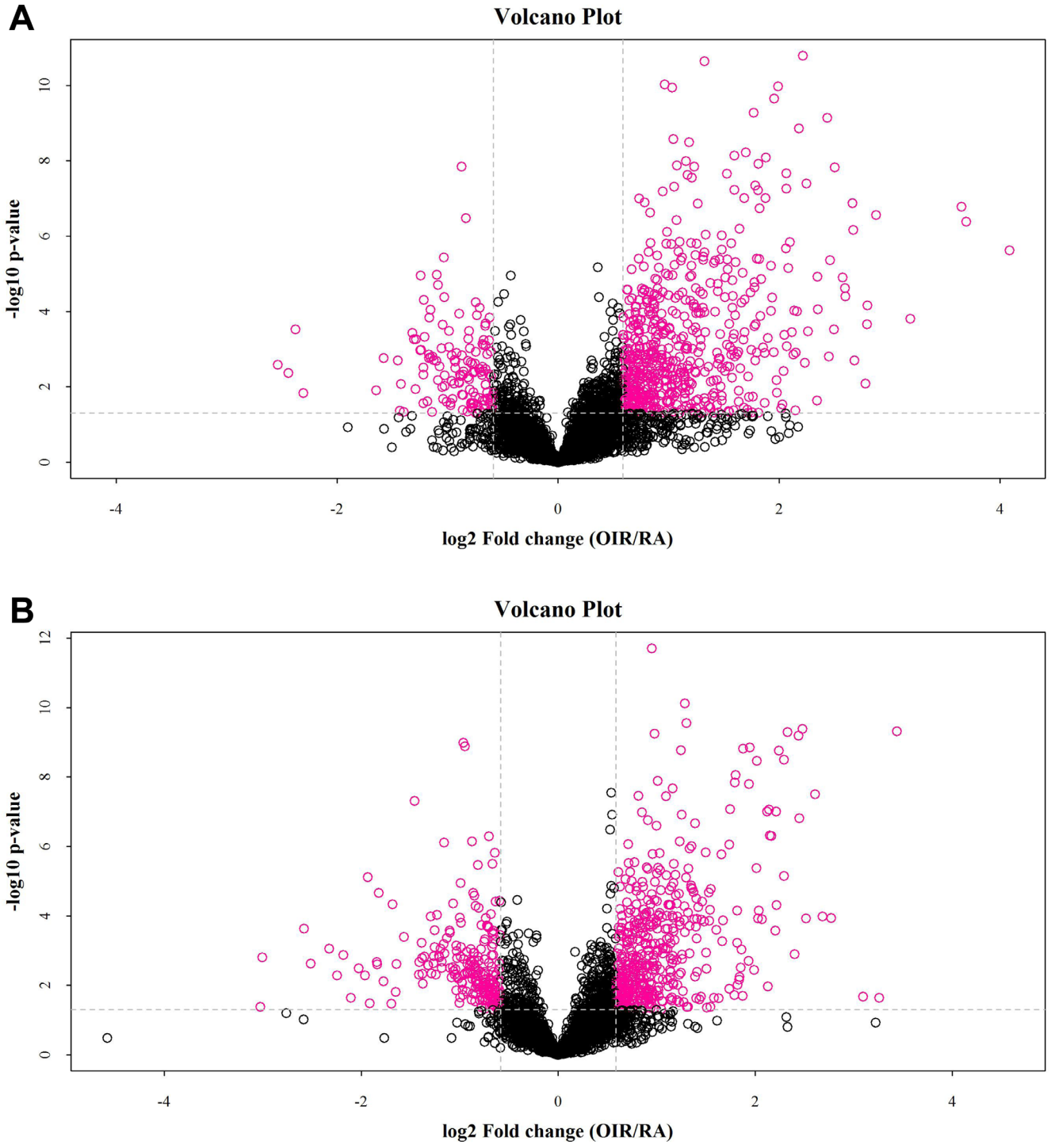

Figure 3. Volcano plot of the untargeted metabolomics according to the criteria (FC > 1.5, $P < 0.05$) in cationic (**A**) and anionic mode (**B**). The *red points* denote metabolites that are significant different by the selection criteria.

met $P < 0.05$) were significantly altered under the anionic mode, including 12 amino acids and their derivatives (Fig. 5, Table 2).

Involved Pathways of Changed Metabolites in OIR Retinas

The KEGG analyses were carried out to discover the involvement of signaling pathways of those altered metabolites. As Figure 6 demonstrated, some essential pathways have been detected. The top 10 enriched pathways are: (1) ATP-binding cassette (ABC) transporters; (2) central carbon metabolism in cancer; (3) alanine, aspartate, and glutamate metabolism; (4) choline metabolism in cancer; (5) synaptic vesicle cycle; (6) protein digestion and absorption; (7) nicotine addiction; (8) taste transduction; (9) aminoacyl-tRNA biosynthesis; and (10) glycerophospholipid metabolism.

Investigative Ophthalmology & Visual Science

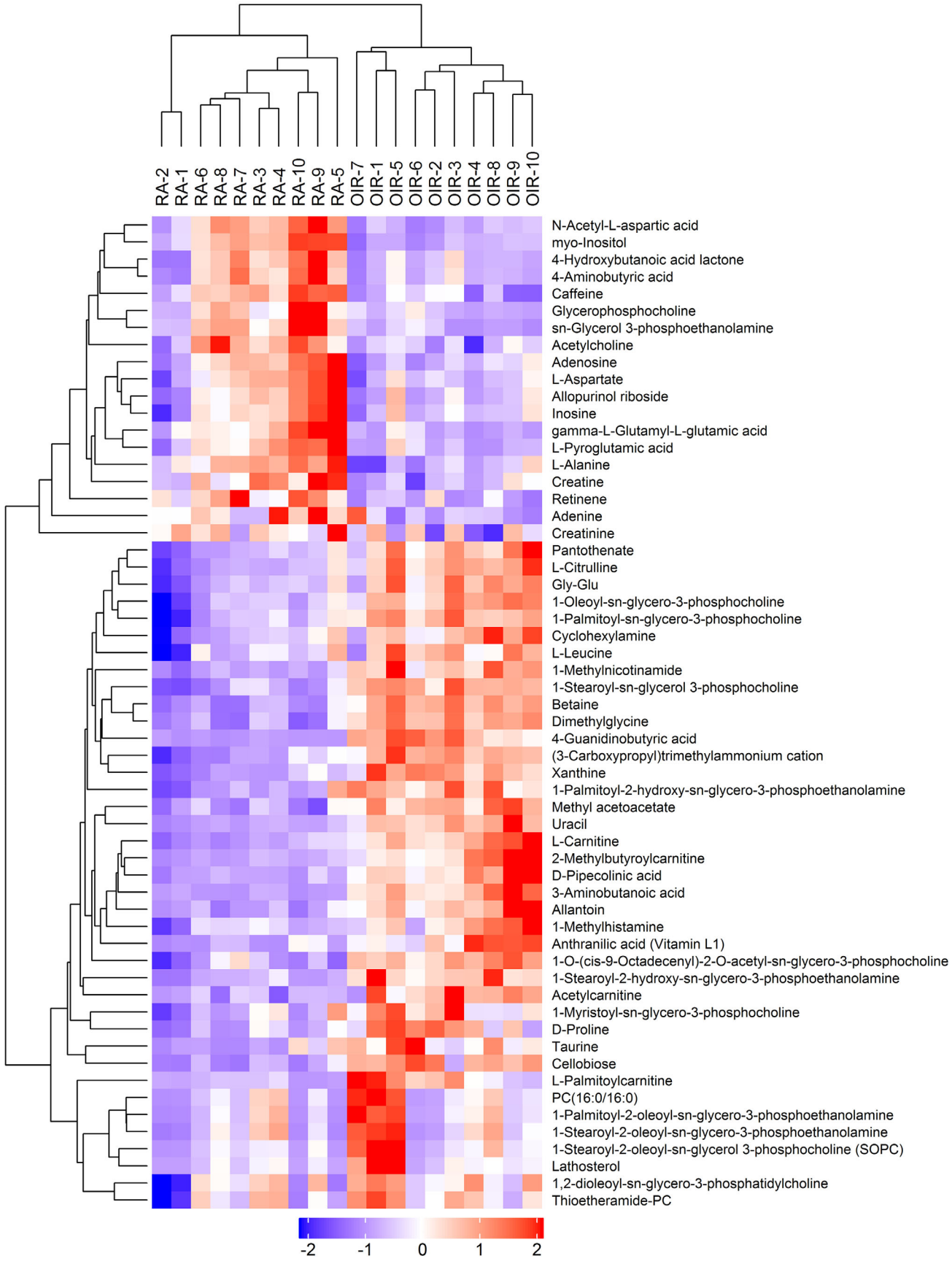

Figure 4. Heatmap of the differential metabolites under the cationic ion mode of untargeted metabolomics. The *blue color* represents low relative level of each metabolite, and the *red color* represents high relative level of each metabolite. Similarly hereinafter in Figure 5 and Figure 7.

Investigative Ophthalmology & Visual Science

Table 1. Significantly Altered Metabolites by Untargeted Metabolomics Under Cationic Mode

Metabolite	VIP	Fold Change	*P* Value	m/z	rt(s)
Betaine	8.953066	2.349001	0.000000	118.08524	510.7
4-Guanidinobutyric acid	3.265833	4.179172	0.000000	146.09125	673.567
Dimethylglycine	1.918242	2.884359	0.000000	104.06937	564.983
1-Stearoyl-sn-glycerol 3-phosphocholine	8.949199	2.402410	0.000000	524.36977	336.257
3-Aminobutanoic acid	1.372053	6.369030	0.000001	104.0694	628.794
Cellobiose	1.204995	2.788409	0.000001	360.14902	749.718
Xanthine	2.173596	2.300530	0.000002	153.03982	395.371
(3-Carboxypropyl)trimethylammonium cation	5.708917	1.786359	0.000002	146.1169	714.139
Methyl acetoacetate	1.046955	2.504663	0.000003	116.04417	339.3485
L-Carnitine	1.525093	2.366309	0.000003	162.11155	719.441
1-O-(cis-9-Octadecenyl)-2-O-acetyl-sn-glycero-3-phosphocholine	1.133253	2.173267	0.000004	550.38401	331.269
1-Methylnicotinamide	1.503464	2.485537	0.000004	137.06985	548.3675
Uracil	4.943300	4.237295	0.000007	113.03348	144.069
Allantoin	1.915934	3.575247	0.000014	159.04983	339.119
L-Citrulline	1.484860	1.858884	0.000014	176.10198	741.18
D-Pipecolinic acid	1.104317	2.719950	0.000018	130.08489	579.57
1-Palmitoyl-sn-glycero-3-phosphocholine	11.308273	1.546523	0.000026	496.33912	361.336
1-Oleoyl-sn-glycero-3-phosphocholine	5.651979	1.698235	0.000032	522.35428	356.527
1-Stearoyl-2-hydroxy-sn-glycero-3-phosphoethanolamine	3.256977	2.130064	0.000037	482.32233	366.758
Myo-Inositol	2.534302	0.489591	0.000042	198.09639	747.817
1-Palmitoyl-2-hydroxy-sn-glycero-3-phosphoethanolamine	2.231755	1.753614	0.000047	454.29152	373.4
2-Methylbutyroylcarnitine	7.609122	3.217040	0.000048	246.16946	445.04
Acetylcarnitine	2.327520	2.344172	0.000074	204.12234	610.7025
N-Acetyl-L-aspartic acid	1.789313	0.600537	0.000126	176.05439	763.209
L-Alanine	1.651170	0.790843	0.000166	90.05378	656.4865
Pantothenate	1.539991	1.835488	0.000169	220.11705	518.703
Gly-Glu	1.744664	1.625211	0.000218	205.08169	811.507
Anthranilic acid (Vitamin L1)	4.130355	4.135162	0.000413	138.05411	535.905
Caffeine	1.487641	0.744461	0.000413	195.08664	81.9335
D-Proline	1.333765	1.502402	0.000504	116.06943	582.18
Sn-Glycerol 3-phosphoethanolamine	1.148223	0.409955	0.000534	216.0624	751.06
Retinene	2.280138	0.679650	0.000890	285.22027	63.458
L-Palmitoylcarnitine	3.637117	3.613271	0.000897	400.34122	321.835
Gamma-L-Glutamyl-L-glutamic acid	3.204750	0.420936	0.001050	277.10234	893.407
1-Methylhistamine	1.212805	1.728684	0.001411	126.10137	628.794
Cyclohexylamine	4.490465	1.425476	0.001995	160.13257	729.001
Acetylcholine	1.161993	0.696391	0.002713	146.11621	349.639
Creatine	1.615463	0.551593	0.003827	132.07554	722.129
Adenosine	2.064261	0.550940	0.004720	285.12732	656.185
L-Pyroglutamic acid	2.245481	0.619670	0.004817	276.11817	830.854
Taurine	1.533283	1.596386	0.005044	126.02064	329.37
L-Leucine	1.185952	1.320973	0.008439	132.10098	490.0545
1-Myristoyl-sn-glycero-3-phosphocholine	1.994833	1.515963	0.009542	468.30755	368.592
Glycerophosphocholine	3.384507	0.482741	0.010195	258.10931	735.46
4-Aminobutyric acid	3.116019	0.731372	0.010626	104.0696	702.929
4-Hydroxybutanoic acid lactone	2.382212	0.724217	0.012970	87.04301	703.082
L-Aspartate	2.339714	0.700536	0.018222	134.04385	773.456
1-Stearoyl-2-oleoyl-sn-glycerol 3-phosphocholine (SOPC)	4.606284	3.106356	0.024919	788.6144	1172.295
Adenine	1.287452	0.601949	0.029236	136.06055	293.579
Allopurinol riboside	4.297267	0.778203	0.037926	537.16755	404.1
Lathosterol	1.314725	3.275910	0.040036	369.35081	1165.38
Thioetheramide-PC	3.237043	1.266703	0.041169	758.56859	269.8885
1,2-Dioleoyl-sn-glycero-3-phosphatidylcholine	3.159002	1.298343	0.055688	786.59934	266.664
1-Palmitoyl-2-oleoyl-sn-glycero-3-phosphoethanolamine	1.172687	2.401201	0.056496	718.53496	1167.655
PC(16:0/16:0)	8.734111	2.382445	0.068061	734.56849	1168.51
1-Stearoyl-2-oleoyl-sn-glycero-3-phosphoethanolamine	1.469349	2.011624	0.073899	746.56768	1172.36
Creatinine	1.364756	0.769696	0.081739	114.06474	312.308
Inosine	3.961990	0.816050	0.088064	269.08745	404.105

Metabolomics Analysis Targeting Amino Acids and their Derivatives

To confirm the reliability of the untargeted metabolomics and explore the metabolomics profiles in key time points of the OIR model, we performed metabolomics analysis targeting amino acids and their derivatives in retinas of OIR mice and room air controls at P12, P13, P17, and P42. The assessed amino acids and their derivatives include 31 metabolites (Fig. 7, Table 3). No significant change was

Investigative Ophthalmology & Visual Science

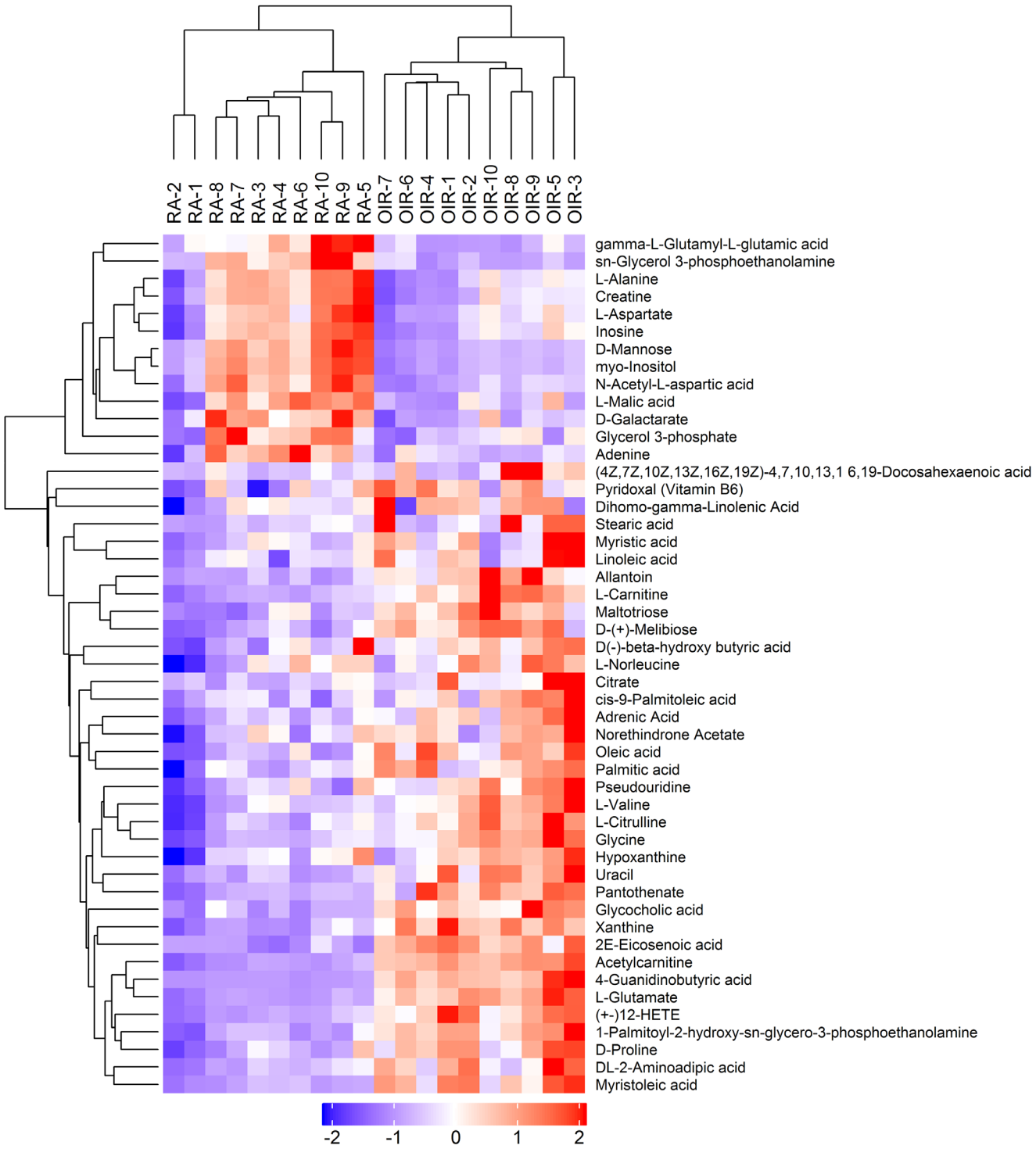

Figure 5. Heatmap of the differential metabolites under the anionic mode of untargeted metabolomics.

found in all of the amino acids and their derivatives at P12 (see Fig. 7A). However, in the early time of hypoxia at P13, 15 metabolites were significantly altered ($P < 0.05$). Among them, eight were increased and seven were decreased, whereas the ranges of fold change were not large (see Fig. 7B). At P17, 19 metabolites were significantly changed in OIR retinas ($P < 0.05$; see Fig. 7C). According to the absolute quantification experiments, only one metabolite (creatine) was significantly decreased, whereas 18 metabolites were significantly increased in retinal tissues of OIR mice. Aminoadipic acid ranked first among the altered amino acids and their derivatives (FC = 3.888804, $P = 0.000000$). Moreover, at the adult time (P42), there are 13 amino acids and their derivatives significantly changed, including only one upregulated metabolite and 12 downregulated metabolites (see Fig. 7D).

Investigative Ophthalmology & Visual Science

Table 2. Significantly Altered Metabolites by Untargeted Metabolomics Under Anionic Mode

Metabolite	VIP	Fold Change	*P* Value	m/z	rt(s)
Acetylcarnitine	1.454661	2.434390	0.000000	262.1294	571.791
L-Glutamate	1.256184	3.821374	0.000000	146.04638	744.064
2E-Eicosenoic acid	1.763247	1.452142	0.000000	309.27977	77.679
4-Guanidinobutyric acid	1.332435	6.088734	0.000000	144.07809	669.805
Xanthine	6.642292	2.346172	0.000001	151.0265	383.609
1-Palmitoyl-2-hydroxy-sn-glycero-3-phosphoethanolamine	2.764355	1.859510	0.000004	452.27722	373.564
(+-)12-HETE	5.306001	2.499252	0.000004	319.22784	84.953
Myristoleic acid	3.118652	2.280041	0.000007	225.18586	83.528
D-(+)-Melibiose	1.337255	2.247703	0.000011	341.10845	746.496
Pantothenate	3.027996	2.547344	0.000013	218.10383	510.606
L-Carnitine	3.258514	2.588557	0.000020	220.11952	664.11
Myo-Inositol	7.340530	0.476325	0.000044	179.05653	743.717
Glycocholic acid	1.003178	1.916077	0.000046	464.31154	349.503
Uracil	6.734364	3.519054	0.000069	111.0201	168.358
D-Mannose	6.975081	0.425147	0.000092	239.07745	743.717
Glycine	3.759812	2.027606	0.000095	74.02505	680.283
Maltotriose	1.052258	2.421338	0.000131	563.18163	865.745
Oleic acid	6.806489	1.759083	0.000132	281.24894	110.021
Allantoin	3.540601	2.890388	0.000137	157.03705	337.978
L-Citrulline	1.403042	1.709572	0.000253	174.08906	739.842
D-Proline	1.742049	1.569806	0.000385	114.05627	576.359
L-Valine	1.587966	1.497543	0.000450	116.07191	560.089
Sn-Glycerol 3-phosphoethanolamine	1.991441	0.382196	0.000586	214.04908	749.794
N-Acetyl-L-aspartic acid	7.576935	0.632832	0.000640	174.04114	764.751
DL-2-Aminoadipic acid	1.089888	2.125641	0.000886	160.06185	787.333
Palmitic acid	8.007681	1.124176	0.001089	255.2332	82.059
Gamma-L-Glutamyl-L-glutamic acid	2.601294	0.416845	0.001448	275.08845	897.509
Adrenic Acid	3.755722	1.267188	0.002212	331.26359	76.565
D-Galactarate	1.787986	0.551609	0.002474	191.01936	286.1585
Pseudouridine	1.141947	1.806677	0.003126	243.06197	447.9605
Creatine	3.540442	0.722911	0.006794	130.06261	652.947
Cis-9-Palmitoleic acid	4.058978	2.240018	0.008495	253.21774	110.293
L-Alanine	3.306320	0.783691	0.014585	88.04076	652.824
Pyridoxal (Vitamin B6)	1.311114	1.586000	0.014743	166.05095	162.597
Norethindrone Acetate	3.483931	1.379377	0.020288	339.19959	83.273
Stearic acid	5.603181	2.729253	0.021242	283.26433	244.98
L-Malic acid	4.072239	0.743349	0.022810	133.01471	783.252
Adenine	1.626748	0.631079	0.024188	134.04716	281.5275
Linoleic acid	2.920425	1.513296	0.025747	279.23299	109.611
Citrate	1.156295	2.222213	0.027596	191.02026	979.294
Glycerol 3-phosphate	1.650010	0.667400	0.030425	171.00679	837.313
Myristic acid	4.788453	1.245557	0.031348	227.20215	83.989
Inosine	10.909695	0.797612	0.034407	267.0736	396.051
Hypoxanthine	4.863956	1.231164	0.036415	135.03152	293.914
L-Aspartate	4.098384	0.741791	0.047288	132.03067	774.182
D(-)-beta-hydroxy butyric acid	1.166855	1.406794	0.056202	103.04025	345.8365
L-Norleucine	2.819077	1.274431	0.060061	130.08762	487.643
Dihomo-gamma-Linolenic Acid	1.376884	1.427861	0.066364	305.24759	119.618
(4Z,7Z,10Z,13Z,16Z,19Z)-4,7,10,13,1 6,19-Docosahexaenoic acid	5.555343	2.162096	0.068306	327.23252	138.446

Discussion

This study primarily screened the metabolomic profile changes in the retinal tissues of OIR mice through untargeted metabolomics analysis and identified a variety of altered metabolites involving in retinal neovascularization (Tables 1, 2). Particularly, numerous amino acids and their derivatives were detected to be significantly altered. Thus, a targeted metabolomics study focusing on amino acids and their derivatives was made to confirm whether those metabolites were significantly changed. As shown in Figure 7 and Table 3, at the time point of P12, when the OIR mice were just removed from the hyperoxia environment, all of the assessed amino acids and their derivatives were not significantly altered. However, 15 and 19 amino acids and their derivatives were found to be significantly changed at P13 and P17, respectively. These findings indicate that the metabolomic alteration of amino acids and their derivatives coincide with the development of retinal angiogenesis. Interestingly, the metabolomic alteration was also found at P42 in the OIR retinas, which suggested that hypoxia-induced angiogenesis could have a long-term impact on the profile of metabolites, it may last even when retinal neovascularization has regressed.

Amino acids and their derivatives are the constituent units of proteins and the most basic substances in life activities.

Investigative Ophthalmology & Visual Science

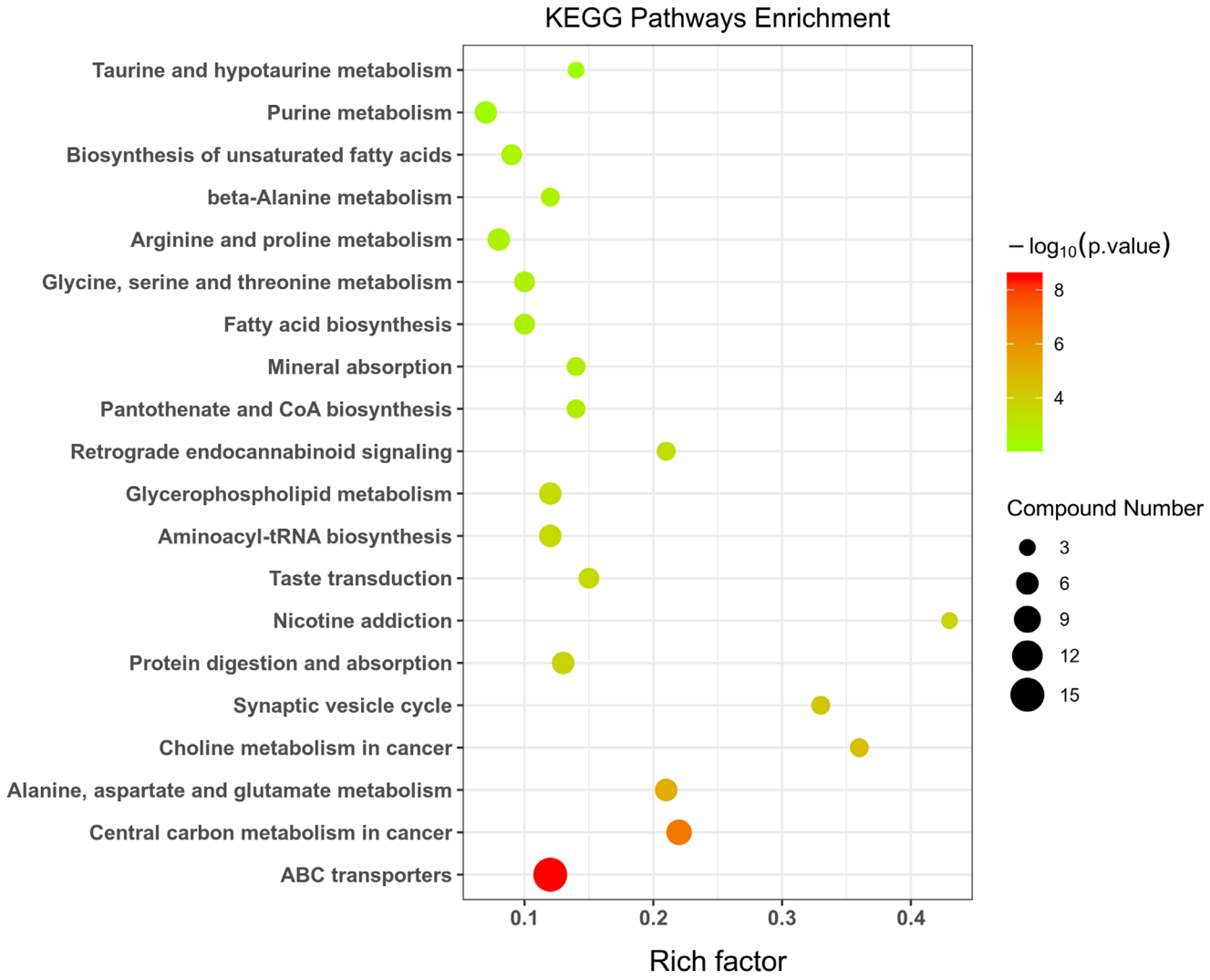

Figure 6. KEGG pathway analysis shows the top 20 involved pathways of significantly altered metabolites. The spot size represents the compound number of metabolites, and the color represents of *P* value.

They play an important role in metabolism, nerve transmission, and liposome transport. Amino acids also participated in the pathogenesis of angiogenesis-related diseases. Liesche et al. demonstrated that ^{18}F-Fluoroethyl-tyrosine uptake was mediated by amino acid transporters in glioblastomas and could be associated with tumor neovascularization.[32] Plasminogen kringle 5 exerted an anti-angiogenic effect when 5 acidic amino acids in the NH2 terminal were replaced by serine residues.[33] Macrophages are angiogenic cells that contribute to diverse functions in ocular neovascular diseases,[34] and M2 macrophages have been demonstrated to enhance pathological neovascular tufts in OIR retinas.[30] Metabolic networks, including amino acids and their derivatives, were involved in macrophage polarization, which may identify novel pharmacologic control targets for both M1 and M2 macrophage phenotypes.[22]

For instance, based on the targeted metabolomics analysis, arginine was upregulated in the retinal tissues of OIR model compared to the controls (see Table 3). Arginine is the precursor of angiogenesis modulator nitric oxide (NO), and arginine deiminase (ADI) was reported to attenuate lipopolysaccharide-induced NO synthesis. ADI inhibited angiogenesis and tumor growth, suppression of angiogenesis by ADI could be reversed by exogenous arginine surplus.[35] It has been reported that the combination of arginine restricted diet can improve the visual acuity of patients with choroidal neovascularization (CNV) after the intravitreal injection of ranibizumab.[36] L-arginine contributed additional effects on exercise-induced angiogenesis possibly by enhancing VEGF expression in the hind-leg muscles and heart.[37] On the other hand, the enhancement of NO synthesis pathway is characteristic of pro-inflammatory M1-like macrophages, whereas the expression of arginase characterizes M2 macrophages, and arginase hydrolyzes arginine to ornithine and urea while limiting the synthesis of NO derived from arginine.[38] Elms et al. indicated that diabetes induced arginase 1 upregulation and was associated with diabetes-induced impairment of retinal blood flow via vascular endothelial cell dysfunction.[39] Arginase 1 was involved in diabetes-induced senescence of retinal endothelial cells, and inhibiting its activity could be a possible therapeutic method in treating diabetic retinopathy by prevention of premature senescence.[40] Therefore, amino acids, such as arginine, might be involved in the pathogenesis of

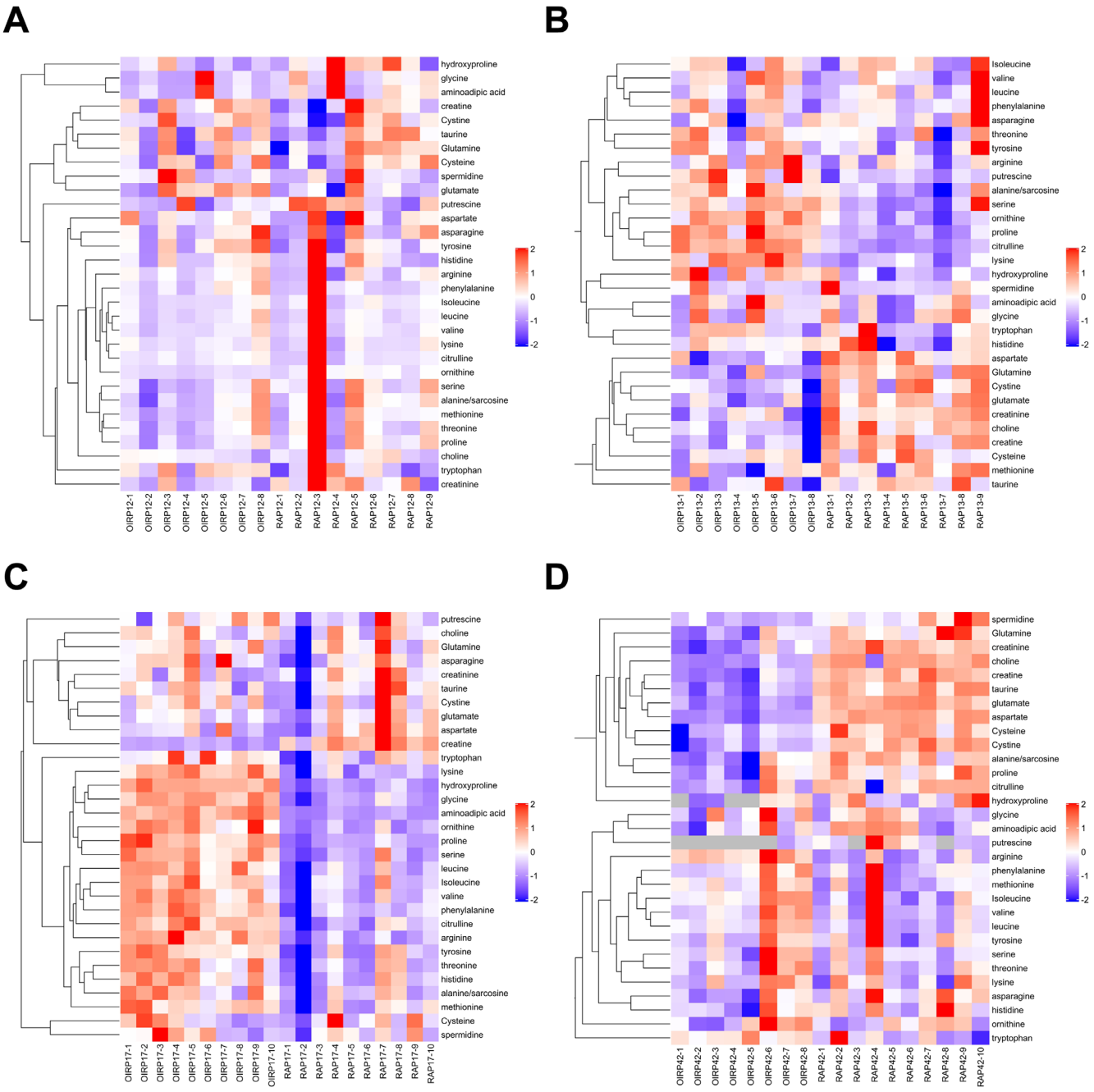

Figure 7. Hierarchical clustering of the amino acids and their derivatives by targeted metabolomics at P12 (**A**), P13 (**B**), P17 (**C**), and P42 (**D**).

angiogenesis-related diseases via regulating macrophage polarization as well as VEGF expression. Nevertheless, further investigations are necessary to reveal the roles and mechanisms of amino acids in ROP and other retinal neovascular diseases.

We recently reported the plasma metabolomic profile of treatment-requiring ROP by assessing clinical samples,[29] combined with the results of the present study, multiple metabolites were significantly changed in the plasma of patients with treatment-requiring ROP as well as the retinal tissues of OIR mice in the present study. For example, caffeine was downregulated in both studies, which supported that caffeine acts as a protective role in the prevention and therapeutics of ROP in previous studies.[41,42] Moreover, similar to the untargeted metabolomics results of the present study, numerous amino acids and their derivatives were significantly altered in the plasma metabolomic profiles of treatment-requiring ROP. This phenomenon indicated the important involvement of amino acid metabolism in retinal neovascularization. Besides, according to the KEGG analyses, some of the pathways involved in the current study were the

Investigative Ophthalmology & Visual Science

Table 3. Screening of Amino Acids and their Derivatives by Targeted Metabolomics Analysis at Key Time Points

Component Name	Analyte Mass Range	P12		P13		P17		P42	
		Fold Change	*P* Value	Fold Change	*P* Value	Fold Change	*P* Value	Fold Change	*P* Value
Alanine/sarcosine	90.1/44.0	0.887558	0.219832	1.098293	0.011347	1.206708	0.017209	0.800972	0.005493
Aminoadipic acid	162.0/98.0	0.704802	0.344725	1.197040	0.313057	3.888804	0.000000	0.851946	0.356745
Arginine	175.1/70.0	0.959192	0.826446	1.111948	0.082967	1.716807	0.000002	1.305738	0.000696
Asparagine	133.1/74.2	1.007225	0.935798	0.940657	0.225575	1.239092	0.195822	0.896267	0.113572
Aspartate	134.0/74.1	1.011729	0.865310	0.869367	0.003592	0.811144	0.252716	0.474227	0.000000
Choline	104.1/60.0	0.932938	0.354552	0.827572	0.001082	1.046199	0.436647	0.667028	0.000033
Citrulline	176.1/159.2	0.852036	0.596496	1.425518	0.000000	1.434105	0.000078	0.753138	0.081236
Creatine	132.1/90.0	1.039047	0.316976	0.849455	0.000764	0.554918	0.000003	0.729565	0.000017
Creatinine	114.1/44.0	0.861490	0.061413	0.779838	0.007370	0.885584	0.374043	0.517874	0.000552
Cysteine	122.1/59.0	1.010753	0.881463	0.918863	0.116909	1.003545	0.985975	0.698304	0.000944
Cystine	241.1/151.9	1.149185	0.373442	0.792629	0.005612	1.065507	0.698526	0.461139	0.000023
Glutamate	148.1/84.1	1.067882	0.090399	0.857977	0.001350	0.791241	0.270533	0.495186	0.000000
Glutamine	147.0/84.1	0.980137	0.749368	0.854234	0.001043	1.045908	0.529621	0.793414	0.004886
Glycine	76.0/30.1	0.732463	0.348047	0.969373	0.848639	1.901860	0.000000	1.107163	0.539125
Histidine	156.1/110.1	0.947756	0.621576	1.017516	0.719063	1.263247	0.003498	0.945161	0.335251
Hydroxyproline	132.1/86.1	0.861915	0.116048	1.284533	0.024508	2.387681	0.000000	0.723812	0.386509
Isoleucine	132.1/86.2	0.790712	0.340765	0.990649	0.860823	1.311220	0.002087	1.209237	0.091206
Leucine	132.1/86.2	0.845454	0.503601	0.972154	0.477898	1.313100	0.000194	1.127586	0.345551
Lysine	147.1/84.0	0.883302	0.552894	1.173240	0.002274	1.545541	0.000010	1.021018	0.651589
Methionine	150.1/133.0	0.883978	0.361231	0.928307	0.061845	1.242132	0.004062	1.115949	0.289352
Ornithine	133.1/70.1	0.646213	0.178437	1.325837	0.000087	1.903014	0.000021	1.037972	0.590842
Phenylalanine	166.1/103.1	0.949986	0.772062	0.980603	0.719073	1.404781	0.000021	1.066927	0.605434
Proline	116.1/70.1	0.825111	0.156605	1.267861	0.000116	1.801760	0.000001	0.846769	0.032768
Putrescine	89.0/72.0	0.774928	0.247170	1.773228	0.003286	1.182088	0.509973	N/A	N/A
Serine	106.0/60.0	0.860040	0.159680	1.099147	0.024818	1.398342	0.000086	1.066454	0.433896
Spermidine	146.2/72.2	1.384154	0.404868	0.690696	0.559895	1.176720	0.352533	0.280345	0.012236
Taurine	126.0/44.1	1.001953	0.969496	0.954156	0.214503	0.987979	0.886926	0.698083	0.000003
Threonine	120.0/74.0	0.884551	0.325620	1.034221	0.290129	1.310529	0.004043	1.071920	0.386383
Tryptophan	205.1/146.3	1.051045	0.504748	0.985433	0.865524	1.233166	0.070158	1.149597	0.191239
Tyrosine	182.1/136.1	1.102028	0.419317	1.048031	0.323769	1.295189	0.004081	1.004620	0.961364
Valine	118.1/72.1	0.802083	0.409696	1.025783	0.532138	1.339369	0.000214	1.087103	0.360184

same as the enriched pathways of the altered plasma metabolites in treatment-requiring ROP infants, such as "ABC transporters," "protein digestion and absorption," "aminoacyl-tRNA biosynthesis," etc. It has been reported that deficiency of amino acid promotes tumor angiogenesis via the pathway of GCN2/ATF4.[43] Similarly, a recent study indicated that the restriction of amino acid induces angiogenesis through the pathway of GCN2/ATF4, and regulates the production of VEGF and H_2S.[44] Moreover, amino acid deprivation induced VEGF expression level in human retinal pigmented epithelial cell line.[45] Therefore, amino acids and their related pathways might play important roles in retinal neovascularization, and further studies are necessary to reveal the functions and mechanisms of amino acid metabolism and those cross-involved pathways in retinal neovascularization.

In conclusion, this study identified metabolomic profile changes in the retinal tissues of OIR mice. By bioinformatics analysis, "ABC transporters," "central carbon metabolism in cancer." and "alanine, aspartate, and glutamate metabolism" were the most enriched KEGG pathways associated with the altered metabolites. Through the screening of the untargeted metabolomics along with the targeted metabolomics analysis, a large number of altered amino acids and their derivatives were detected. These results indicated that metabolites, especially amino acids and their derivatives, together with the involved metabolic pathways, might be involved during the pathological process of retinal neovascular diseases.

Acknowledgments

Supported by the National Natural Science Foundation of China (No. 81800855 and 82070967), Natural Science Foundation of Hunan Province (No. 2020JJ4788), and Changsha Science and Technology Project (No. kq1907075).

Disclosure: **Y. Zhou**, None; **W. Tan**, None; **J. Zou**, None; **J. Cao**, None; **Q. Huang**, None; **B. Jiang**, None; **S. Yoshida**, None; **Y. Li**, None

References

1. Yoshida A, Yoshida S, Ishibashi T, Inomata H. Intraocular neovascularization. *Histol Histopathol*. 1999;14:1287–1294.
2. Pham B, Thomas SM, Lillie E, et al. Anti-vascular endothelial growth factor treatment for retinal conditions: a systematic review and meta-analysis. *BMJ Open*. 2019;9:e022031.
3. Porta M, Striglia E. Intravitreal anti-VEGF agents and cardiovascular risk. *Intern Emerg Med*. 2020;15:199–210.
4. Schargus M, Frings A. Issues with Intravitreal Administration of Anti-VEGF Drugs. *Clin Ophthalmol*. 2020;14:897–904.
5. Zhang L, Fu X, Zeng H, et al. Microarray Analysis of Long Non-Coding RNAs and Messenger RNAs in a Mouse Model of Oxygen-Induced Retinopathy. *Int J Med Sci*. 2019;16:537–547.
6. Connor KM, Krah NM, Dennison RJ, et al. Quantification of oxygen-induced retinopathy in the mouse: a model of

vessel loss, vessel regrowth and pathological angiogenesis. *Nat Protoc*. 2009;4:1565–1573.

7. Amin S, Gonzalez A, Guevara J, et al. Efficacy of Aflibercept Treatment and its Effect on the Retinal Perfusion in the Oxygen-Induced Retinopathy Mouse Model of Retinopathy of Prematurity. *Ophthalmic Res*. 2020;64(1):91–98.
8. Zhang LS, Zhou YD, Peng YQ, Zeng HL, Yoshida S, Zhao TT. Identification of altered microRNAs in retinas of mice with oxygen-induced retinopathy. *Int J Ophthalmol*. 2019;12:739–745.
9. Cao M, Zhang L, Wang JH, et al. Identifying circRNA-associated-ceRNA networks in retinal neovascularization in mice. *Int J Med Sci*. 2019;16:1356–1365.
10. Peng Y, Zou J, Wang JH, et al. Small RNA Sequencing Reveals Transfer RNA-derived Small RNA Expression Profiles in Retinal Neovascularization. *Int J Med Sci*. 2020;17:1713–1722.
11. Vahatupa M, Nattinen J, Jylha A, et al. SWATH-MS Proteomic Analysis of Oxygen-Induced Retinopathy Reveals Novel Potential Therapeutic Targets. *Invest Ophthalmol Vis Sci*. 2018;59:3294–3306.
12. Kim SJ, Jin J, Kim YJ, Kim Y, Yu HG. Retinal proteome analysis in a mouse model of oxygen-induced retinopathy. *J Proteome Res*. 2012;11:5186–5203.
13. Vahatupa M, Jarvinen TAH, Uusitalo-Jarvinen H. Exploration of Oxygen-Induced Retinopathy Model to Discover New Therapeutic Drug Targets in Retinopathies. *Front Pharmacol*. 2020;11:873.
14. Juppner J, Mubeen U, Leisse A, et al. Dynamics of lipids and metabolites during the cell cycle of Chlamydomonas reinhardtii. *Plant J*. 2017;92:331–343.
15. Li Q, Wei S, Wu D, Wen C, Zhou J. Urinary Metabolomics Study of Patients with Gout Using Gas Chromatography-Mass Spectrometry. *Biomed Res Int*. 2018;2018:3461572.
16. Armitage EG, Barbas C. Metabolomics in cancer biomarker discovery: current trends and future perspectives. *J Pharm Biomed Anal*. 2014;87:1–11.
17. Humer E, Pieh C, Probst T. Metabolomic Biomarkers in Anxiety Disorders. *Int J Mol Sci*. 2020;21(13):4784.
18. Lv H, Jiang F, Guan D, et al. Metabolomics and Its Application in the Development of Discovering Biomarkers for Osteoporosis Research. *Int J Mol Sci*. 2016;17(12):2018.
19. Luo Y, Cui HP, Liu Y, Chen L. Metabolomics and biomarkers in ocular matrix: beyond ocular diseases. *Int J Ophthalmol*. 2020;13:991–1003.
20. Williams C, Palviainen M, Reichardt NC, Siljander PR, Falcon-Perez JM. Metabolomics Applied to the Study of Extracellular Vesicles. *Metabolites*. 2019;9(11):276.
21. Troisi J, Cavallo P, Colucci A, et al. Metabolomics in genetic testing. *Adv Clin Chem*. 2020;94:85–153.
22. Jha AK, Huang SC, Sergushichev A, et al. Network integration of parallel metabolic and transcriptional data reveals metabolic modules that regulate macrophage polarization. *Immunity*. 2015;42:419–430.
23. Sumarriva K, Uppal K, Ma C, et al. Arginine and Carnitine Metabolites Are Altered in Diabetic Retinopathy. *Invest Ophthalmol Vis Sci*. 2019;60:3119–3126.
24. Wei P, He M, Teng H, Han G. Metabolomic analysis of the aqueous humor from patients with central retinal vein occlusion using UHPLC-MS/MS. *J Pharm Biomed Anal*. 2020;188:113448.
25. Chen L, Chang R, Pan S, et al. Plasma metabolomics study of Vogt-Koyanagi-Harada disease identifies potential diagnostic biomarkers. *Exp Eye Res*. 2020;196:108070.
26. Bonelli R, Woods SM, Ansell BRE, et al. Systemic lipid dysregulation is a risk factor for macular neurodegenerative disease. *Sci Rep*. 2020;10:12165.
27. Han G, Wei P, He M, Teng H, Chu Y. Metabolomic Profiling of the Aqueous Humor in Patients with Wet Age-Related Macular Degeneration Using UHPLC-MS/MS. *J Proteome Res*. 2020;19:2358–2366.
28. Lu F, Liu Y, Guo Y, et al. Metabolomic changes of blood plasma associated with two phases of rat OIR. *Exp Eye Res*. 2020;190:107855.
29. Zhou Y, Xu Y, Zhang X, et al. Plasma metabolites in treatment-requiring retinopathy of prematurity: Potential biomarkers identified by metabolomics. *Exp Eye Res*. 2020;199:108198.
30. Zhou Y, Yoshida S, Nakao S, et al. M2 Macrophages Enhance Pathological Neovascularization in the Mouse Model of Oxygen-Induced Retinopathy. *Invest Ophthalmol Vis Sci*. 2015;56:4767–4777.
31. Cai Y, Weng K, Guo Y, Peng J, Zhu Z-J. An integrated targeted metabolomic platform for high-throughput metabolite profiling and automated data processing. *Metabolomics*. 2015;11:1575–1586.
32. Liesche F, Lukas M, Preibisch C, et al. (18)F-Fluoroethyltyrosine uptake is correlated with amino acid transport and neovascularization in treatment-naive glioblastomas. *Eur J Nucl Med Mol Imaging*. 2019;46:2163–2168.
33. Li C, Li L, Cheng R, et al. Acidic/neutral amino acid residues substitution in NH2 terminal of plasminogen kringle 5 exerts enhanced effects on corneal neovascularization. *Cornea*. 2013;32:680–688.
34. Zhou YD, Yoshida S, Peng YQ, Kobayashi Y, Zhang LS, Tang LS. Diverse roles of macrophages in intraocular neovascular diseases: a review. *Int J Ophthalmol*. 2017;10:1902–1908.
35. Park IS, Kang SW, Shin YJ, et al. Arginine deiminase: a potential inhibitor of angiogenesis and tumour growth. *Br J Cancer*. 2003;89:907–914.
36. Chatziralli I, Theodossiadis G, Emfietzoglou I, Theodossiadis P. Intravitreal ranibizumab for choroidal neovascularization secondary to gyrate atrophy in a young patient: a multimodal imaging analysis. *Eur J Ophthalmol*. 2015;25:e119–e122.
37. Suzuki J. L-arginine supplementation causes additional effects on exercise-induced angiogenesis and VEGF expression in the heart and hind-leg muscles of middle-aged rats. *J Physiol Sci*. 2006;56:39–44.
38. Netea-Maier RT, Smit JWA, Netea MG. Metabolic changes in tumor cells and tumor-associated macrophages: A mutual relationship. *Cancer Lett*. 2018;413:102–109.
39. Elms SC, Toque HA, Rojas M, Xu Z, Caldwell RW, Caldwell RB. The role of arginase I in diabetes-induced retinal vascular dysfunction in mouse and rat models of diabetes. *Diabetologia*. 2013;56:654–662.
40. Shosha E, Xu Z, Narayanan SP, et al. Mechanisms of Diabetes-Induced Endothelial Cell Senescence: Role of Arginase 1. *Int J Mol Sci*. 2018;19(4):1215.
41. Zhang S, Zhou R, Li B, et al. Caffeine preferentially protects against oxygen-induced retinopathy. *FASEB J*. 2017;31:3334–3348.
42. Chen JF, Zhang S, Zhou R, et al. Adenosine receptors and caffeine in retinopathy of prematurity. *Mol Aspects Med*. 2017;55:118–125.
43. Wang Y, Ning Y, Alam GN, et al. Amino acid deprivation promotes tumor angiogenesis through the GCN2/ATF4 pathway. *Neoplasia*. 2013;15:989–997.
44. Longchamp A, Mirabella T, Arduini A, et al. Amino Acid Restriction Triggers Angiogenesis via GCN2/ATF4 Regulation of VEGF and H2S Production. *Cell*. 2018;173:117–129.e14.
45. Abcouwer SF, Marjon PL, Loper RK, Vander Jagt DL. Response of VEGF expression to amino acid deprivation and inducers of endoplasmic reticulum stress. *Invest Ophthalmol Vis Sci*. 2002;43:2791–2798.

Investigative Ophthalmology & Visual Science